

Pion femtoscopy in $p + p$ collisions at $\sqrt{s} = 200$ GeV

B. I. Abelev,⁸ M. M. Aggarwal,³¹ Z. Ahammed,⁴⁸ A. V. Alakhverdyants,¹⁸ I. Alekseev,¹⁶ B. D. Anderson,¹⁹ D. Arkhipkin,³
 G. S. Averichev,¹⁸ J. Balewski,²³ L. S. Barnby,² S. Baumgart,⁵³ D. R. Beavis,³ R. Bellwied,⁵¹ F. Benedosso,²⁸
 M. J. Betancourt,²³ R. R. Betts,⁸ A. Bhasin,¹⁷ A. K. Bhati,³¹ H. Bichsel,⁵⁰ J. Bielcik,¹⁰ J. Bielcikova,¹¹ B. Biritz,⁶
 L. C. Bland,³ B. E. Bonner,³⁷ J. Bouchet,¹⁹ E. Braidot,²⁸ A. V. Brandin,²⁶ A. Bridgeman,¹ E. Bruna,⁵³ S. Bueltmann,³⁰
 I. Bunzarov,¹⁸ T. P. Burton,³ X. Z. Cai,⁴¹ H. Caines,⁵³ M. Calderón de la Barca Sánchez,⁵ O. Catu,⁵³ D. Cebra,⁵ R. Cendejas,⁶
 M. C. Cervantes,⁴³ Z. Chajecski,²⁹ P. Chaloupka,¹¹ S. Chattopadhyay,⁴⁸ H. F. Chen,³⁹ J. H. Chen,⁴¹ J. Y. Chen,⁵² J. Cheng,⁴⁵
 M. Cherney,⁹ A. Chikanian,⁵³ K. E. Choi,³⁵ W. Christie,³ P. Chung,¹¹ R. F. Clarke,⁴³ M. J. M. Coddington,⁴³ R. Corliss,²³
 J. G. Cramer,⁵⁰ H. J. Crawford,⁴ D. Das,⁵ S. Dash,¹³ A. Davila Leyva,⁴⁴ L. C. De Silva,⁵¹ R. R. Debbé,³ T. G. Dedovich,¹⁸
 M. DePhillips,³ A. A. Derevschikov,³³ R. Derradi de Souza,⁷ L. Didenko,³ P. Djawotho,⁴³ S. M. Dogra,¹⁷ X. Dong,²²
 J. L. Drachenberg,⁴³ J. E. Draper,⁵ J. C. Dunlop,³ M. R. Dutta Mazumdar,⁴⁸ L. G. Efimov,¹⁸ E. Elhalhuli,² M. Elnimr,⁵¹
 J. Engelage,⁴ G. Eppley,³⁷ B. Erazmus,⁴² M. Estienne,⁴² L. Eun,³² O. Evdokimov,⁸ P. Fachini,³ R. Fatemi,²⁰ J. Fedorisin,¹⁸
 R. G. Fersch,²⁰ P. Filip,¹⁸ E. Finch,⁵³ V. Fine,³ Y. Fisyak,³ C. A. Gagliardi,⁴³ D. R. Gangadharan,⁶ M. S. Ganti,⁴⁸
 E. J. Garcia-Solis,⁸ A. Geromitsos,⁴² F. Geurts,³⁷ V. Ghazikhanian,⁶ P. Ghosh,⁴⁸ Y. N. Gorbunov,⁹ A. Gordon,³
 O. Grebenyuk,²² D. Grosnick,⁴⁷ B. Grube,³⁵ S. M. Guertin,⁶ A. Gupta,¹⁷ N. Gupta,¹⁷ W. Guryn,³ B. Haag,⁵ A. Hamed,⁴³
 L.-X. Han,⁴¹ J. W. Harris,⁵³ J. P. Hays-Wehle,²³ M. Heinz,⁵³ S. Heppelmann,³² A. Hirsch,³⁴ E. Hjort,²² A. M. Hoffman,²³
 G. W. Hoffmann,⁴⁴ D. J. Hofman,⁸ R. S. Hollis,⁸ H. Z. Huang,⁶ T. J. Humanic,²⁹ L. Huo,⁴³ G. Igo,⁶ A. Iordanova,⁸ P. Jacobs,²²
 W. W. Jacobs,¹⁵ P. Jakl,¹¹ C. Jena,¹³ F. Jin,⁴¹ C. L. Jones,²³ P. G. Jones,² J. Joseph,¹⁹ E. G. Judd,⁴ S. Kabana,⁴² K. Kajimoto,⁴⁴
 K. Kang,⁴⁵ J. Kapitan,¹¹ K. Kauder,⁸ D. Keane,¹⁹ A. Kechechyan,¹⁸ D. Kettler,⁵⁰ D. P. Kikola,²² J. Kiryluk,²² A. Kisiel,⁴⁹
 S. R. Klein,²² A. G. Knospé,⁵³ A. Kocoloski,²³ D. D. Koetke,⁴⁷ T. Kollegger,¹² J. Konzer,³⁴ M. Kopytine,¹⁹ I. Koralt,³⁰
 L. Koroleva,¹⁶ W. Korsch,²⁰ L. Kotchenda,²⁶ V. Kouchpil,¹¹ P. Kravtsov,²⁶ K. Krueger,¹ M. Krus,¹⁰ L. Kumar,³¹ P. Kurnadi,⁶
 M. A. C. Lamont,³ J. M. Landgraf,³ S. LaPointe,⁵¹ J. Lauret,³ A. Lebedev,³ R. Lednicky,¹⁸ C.-H. Lee,³⁵ J. H. Lee,³ W. Leight,²³
 M. J. LeVine,³ C. Li,³⁹ L. Li,⁴⁴ N. Li,⁵² W. Li,⁴¹ X. Li,⁴⁰ X. Li,³⁴ Y. Li,⁴⁵ Z. Li,⁵² G. Lin,⁵³ S. J. Lindenbaum,²⁷ M. A. Lisa,²⁹
 F. Liu,⁵² H. Liu,⁵ J. Liu,³⁷ T. Ljubicic,³ W. J. Llope,³⁷ R. S. Longacre,³ W. A. Love,³ Y. Lu,³⁹ G. L. Ma,⁴¹ Y. G. Ma,⁴¹
 D. P. Mahapatra,¹³ R. Majka,⁵³ O. I. Mall,⁵ L. K. Mangotra,¹⁷ R. Manweiler,⁴⁷ S. Margetis,¹⁹ C. Markert,⁴⁴ H. Masui,²²
 H. S. Matis,²² Yu. A. Matulenko,³³ D. McDonald,³⁷ T. S. McShane,⁹ A. Meschanin,³³ R. Milner,²³ N. G. Minaev,³³
 S. Mioduszewski,⁴³ A. Mischke,²⁸ M. K. Mitrovski,¹² B. Mohanty,⁴⁸ M. M. Mondal,⁴⁸ B. Morozov,¹⁶ D. A. Morozov,³³
 M. G. Munhoz,³⁸ B. K. Nandi,¹⁴ C. Nattrass,⁵³ T. K. Nayak,⁴⁸ J. M. Nelson,² P. K. Netrakanti,³⁴ M. J. Ng,⁴ L. V. Nogach,³³
 S. B. Nurushev,³³ G. Odyniec,²² A. Ogawa,³ H. Okada,³ V. Okorokov,²⁶ D. Olson,²² M. Pachr,¹⁰ B. S. Page,¹⁵ S. K. Pal,⁴⁸
 Y. Pandit,¹⁹ Y. Panebratsev,¹⁸ T. Pawlak,⁴⁹ T. Peitzmann,²⁸ V. Perevoztchikov,³ C. Perkins,⁴ W. Peryt,⁴⁹ S. C. Phatak,¹³
 P. Pile,³ M. Planinic,⁵⁴ M. A. Ploskon,²² J. Pluta,⁴⁹ D. Plyku,³⁰ N. Poljak,⁵⁴ A. M. Poskanzer,²² B. V. K. S. Potukuchi,¹⁷
 C. B. Powell,²² D. Prindle,⁵⁰ C. Pruneau,⁵¹ N. K. Pruthi,³¹ P. R. Pujahari,¹⁴ J. Putschke,⁵³ R. Raniwala,³⁶ S. Raniwala,³⁶
 R. L. Ray,⁴⁴ R. Redwine,²³ R. Reed,⁵ J. M. Rehberg,¹² H. G. Ritter,²² J. B. Roberts,³⁷ O. V. Rogachevskiy,¹⁸ J. L. Romero,⁵
 A. Rose,²² C. Roy,⁴² L. Ruan,³ M. J. Russcher,²⁸ R. Sahoo,⁴² S. Sakai,⁶ I. Sakrejda,²² T. Sakuma,²³ S. Salur,⁵ J. Sandweiss,⁵³
 E. Sangaline,⁵ J. Schambach,⁴⁴ R. P. Scharenberg,³⁴ N. Schmitz,²⁴ T. R. Schuster,¹² J. Seele,²³ J. Seger,⁹ I. Selyuzhenkov,¹⁵
 P. Seyboth,²⁴ E. Shahaliev,¹⁸ M. Shao,³⁹ M. Sharma,⁵¹ S. S. Shi,⁵² E. P. Sichtermann,²² F. Simon,²⁴ R. N. Singaraju,⁴⁸
 M. J. Skoby,³⁴ N. Smirnov,⁵³ P. Sorensen,³ J. Sowinski,¹⁵ H. M. Spinka,¹ B. Srivastava,³⁴ T. D. S. Stanislaus,⁴⁷
 D. Staszak,⁶ J. R. Stevens,¹⁵ R. Stock,¹² M. Strikhanov,²⁶ B. Stringfellow,³⁴ A. A. P. Suaide,³⁸ M. C. Suarez,⁸
 N. L. Subba,¹⁹ M. Sumbera,¹¹ X. M. Sun,²² Y. Sun,³⁹ Z. Sun,²¹ B. Surrow,²³ D. N. Svirida,¹⁶ T. J. M. Symons,²²
 A. Szanto de Toledo,³⁸ J. Takahashi,⁷ A. H. Tang,³ Z. Tang,³⁹ L. H. Tarini,⁵¹ T. Tarnowsky,²⁵ D. Thein,⁴⁴ J. H. Thomas,²²
 J. Tian,⁴¹ A. R. Timmins,⁵¹ S. Timoshenko,²⁶ D. Tlusty,¹¹ M. Tokarev,¹⁸ T. A. Trainor,⁵⁰ V. N. Tram,²² S. Trentalange,⁶
 R. E. Tribble,⁴³ O. D. Tsai,⁶ J. Ulery,³⁴ T. Ullrich,³ D. G. Underwood,¹ G. Van Buren,³ G. van Nieuwenhuizen,²³
 J. A. Vanfossen, Jr.,¹⁹ R. Varma,¹⁴ G. M. S. Vasconcelos,⁷ A. N. Vasiliev,³³ F. Videbaek,³ Y. P. Vijoyi,⁴⁸ S. Vokal,¹⁸
 S. A. Voloshin,⁵¹ M. Wada,⁴⁴ M. Walker,²³ F. Wang,³⁴ G. Wang,⁶ H. Wang,²⁵ J. S. Wang,²¹ Q. Wang,³⁴ X. L. Wang,³⁹
 Y. Wang,⁴⁵ G. Webb,²⁰ J. C. Webb,³ G. D. Westfall,²⁵ C. Whitten Jr.,⁶ H. Wieman,²² E. Wingfield,⁴⁴ S. W. Wissink,¹⁵
 R. Witt,⁴⁶ Y. Wu,⁵² W. Xie,³⁴ N. Xu,²² Q. H. Xu,⁴⁰ W. Xu,⁶ Y. Xu,³⁹ Z. Xu,³ L. Xue,⁴¹ Y. Yang,²¹ P. Yepes,³⁷ K. Yip,³
 I.-K. Yoo,³⁵ Q. Yue,⁴⁵ M. Zawisza,⁴⁹ H. Zbroszczyk,⁴⁹ W. Zhan,²¹ S. Zhang,⁴¹ W. M. Zhang,¹⁹ X. P. Zhang,²² Y. Zhang,²²
 Z. P. Zhang,³⁹ J. Zhao,⁴¹ C. Zhong,⁴¹ J. Zhou,³⁷ W. Zhou,⁴⁰ X. Zhu,⁴⁵ Y. H. Zhu,⁴¹ R. Zoulkarneev,¹⁸ and Y. Zoulkarneeva¹⁸

(STAR Collaboration)

¹Argonne National Laboratory, Argonne, Illinois 60439, USA²University of Birmingham, Birmingham, United Kingdom

- 52 ³Brookhaven National Laboratory, Upton, New York 11973, USA
53 ⁴University of California, Berkeley, California 94720, USA
54 ⁵University of California, Davis, California 95616, USA
55 ⁶University of California, Los Angeles, California 90095, USA
56 ⁷Universidade Estadual de Campinas, Sao Paulo, Brazil
57 ⁸University of Illinois at Chicago, Chicago, Illinois 60607, USA
58 ⁹Creighton University, Omaha, Nebraska 68178, USA
59 ¹⁰Czech Technical University in Prague, FNSPE, Prague, 115 19, Czech Republic
60 ¹¹Nuclear Physics Institute AS CR, 250 68 Řež/Prague, Czech Republic
61 ¹²University of Frankfurt, Frankfurt, Germany
62 ¹³Institute of Physics, Bhubaneswar 751005, India
63 ¹⁴Indian Institute of Technology, Mumbai, India
64 ¹⁵Indiana University, Bloomington, Indiana 47408, USA
65 ¹⁶Alikhanov Institute for Theoretical and Experimental Physics, Moscow, Russia
66 ¹⁷University of Jammu, Jammu 180001, India
67 ¹⁸Joint Institute for Nuclear Research, Dubna, 141 980, Russia
68 ¹⁹Kent State University, Kent, Ohio 44242, USA
69 ²⁰University of Kentucky, Lexington, Kentucky, 40506-0055, USA
70 ²¹Institute of Modern Physics, Lanzhou, China
71 ²²Lawrence Berkeley National Laboratory, Berkeley, California 94720, USA
72 ²³Massachusetts Institute of Technology, Cambridge, MA 02139-4307, USA
73 ²⁴Max-Planck-Institut für Physik, Munich, Germany
74 ²⁵Michigan State University, East Lansing, Michigan 48824, USA
75 ²⁶Moscow Engineering Physics Institute, Moscow Russia
76 ²⁷City College of New York, New York City, New York 10031, USA
77 ²⁸NIKHEF and Utrecht University, Amsterdam, The Netherlands
78 ²⁹Ohio State University, Columbus, Ohio 43210, USA
79 ³⁰Old Dominion University, Norfolk, VA, 23529, USA
80 ³¹Panjab University, Chandigarh 160014, India
81 ³²Pennsylvania State University, University Park, Pennsylvania 16802, USA
82 ³³Institute of High Energy Physics, Protvino, Russia
83 ³⁴Purdue University, West Lafayette, Indiana 47907, USA
84 ³⁵Pusan National University, Pusan, Republic of Korea
85 ³⁶University of Rajasthan, Jaipur 302004, India
86 ³⁷Rice University, Houston, Texas 77251, USA
87 ³⁸Universidade de Sao Paulo, Sao Paulo, Brazil
88 ³⁹University of Science & Technology of China, Hefei 230026, China
89 ⁴⁰Shandong University, Jinan, Shandong 250100, China
90 ⁴¹Shanghai Institute of Applied Physics, Shanghai 201800, China
91 ⁴²SUBATECH, Nantes, France
92 ⁴³Texas A&M University, College Station, Texas 77843, USA
93 ⁴⁴University of Texas, Austin, Texas 78712, USA
94 ⁴⁵Tsinghua University, Beijing 100084, China
95 ⁴⁶United States Naval Academy, Annapolis, MD 21402, USA
96 ⁴⁷Valparaiso University, Valparaiso, Indiana 46383, USA
97 ⁴⁸Variable Energy Cyclotron Centre, Kolkata 700064, India
98 ⁴⁹Warsaw University of Technology, Warsaw, Poland
99 ⁵⁰University of Washington, Seattle, Washington 98195, USA
100 ⁵¹Wayne State University, Detroit, Michigan 48201, USA
101 ⁵²Institute of Particle Physics, CCNU (HZNU), Wuhan 430079, China
102 ⁵³Yale University, New Haven, Connecticut 06520, USA
103 ⁵⁴University of Zagreb, Zagreb, HR-10002, Croatia
104 (Dated: March 27, 2010)

The STAR Collaboration at RHIC has measured two-pion correlation functions from $p + p$ collisions at $\sqrt{s} = 200$ GeV. Spatial scales are extracted via a femtoscopic analysis of the correlations, though this analysis is complicated by the presence of strong non-femtoscopic effects. Our results are put into the context of the world dataset of femtoscopy in hadron-hadron collisions. We present the first direct comparison of femtoscopy in $p + p$ and heavy ion collisions, under identical analysis and detector conditions.

105 I. INTRODUCTION AND MOTIVATION

106 The experimental program of the Relativistic Heavy Ion
107 Collider (RHIC) at Brookhaven National Laboratory probes

108 Quantum Chromodynamics (QCD) from numerous direc-
109 tions. The extraordinary flexibility of the machine permits
collisions between heavy and light ions at record energies (up

to $\sqrt{s} = 200$ GeV), polarized and unpolarized protons, and strongly asymmetric systems such as $d + \text{Au}$. The proton collisions are the focus of an intense program exploring the spin structure of the nucleon. However, these collisions also serve as a critical “baseline” measurement for the heavy ion physics program that drove the construction of RHIC.

Studies of ultrarelativistic heavy ion collisions aim to explore the equation of state of strongly interacting matter. The highly dynamic nature of the collisions, however, does not allow a purely statistical study of static matter as one might perform in condensed matter physics, but rather requires a detailed understanding of the dynamics itself. If a bulk, self-interacting system is formed (something that should not be assumed *a priori*), the equation of state then plays the dynamic role of generating pressure gradients that drive the collective expansion of the system. Copious evidence [1–4] indicates that a self-interacting system is, in fact, generated in these collisions. The dynamics of the bulk medium is reflected in the transverse momentum (p_T) distribution [5, 6] and momentum-space anisotropy (e.g. “elliptic flow”) [7, 8] of identified particles at low p_T . These observables are well-described in a hydrodynamic scenario, in which a nearly perfect (i.e. very low viscosity) fluid expands explosively under the action of pressure gradients induced by the collision [9].

Two-particle femtoscopy [10] (often called “HBT” analysis) measures the space-time substructure of the emitting source at “freeze-out,” the point at which particles decouple from the system [e.g. 11]. Femtosopic measurements play a special role in understanding bulk dynamics in heavy ion collisions, for several reasons. Firstly, collective flow generates characteristic space-momentum patterns at freezeout that are revealed [11] in the momentum-dependence of pion “HBT radii” (discussed below), the transverse mass dependence of homogeneity lengths [12], and non-identical particle correlations [10, 13]. Secondly, while a simultaneous description of particle-identified p_T distributions, elliptic flow and femtosopic measurements is easily achieved in flow-dominated toy models [e.g. 6], achieving the same level of agreement in a realistic transport calculation is considerably more challenging. In particular, addressing this “HBT puzzle” [14] has led to a deeper understanding of the freezeout hypersurface, collectivity in the initial stage, and the equation of state. Femtosopic signals of long dynamical timescales expected for a system undergoing a first-order phase transition [15, 16], have not been observed [11], providing early evidence that the system at RHIC evolves from QGP to hadron gas via a crossover [17]. This sensitive and unique connection to important underlying physics has motivated a huge systematic study of femtosopic measurements in heavy ion collisions over the past quarter-century [11].

HBT correlations from hadron (e.g. $p + p$) and lepton (e.g. $e^+ + e^-$) collisions have been extensively studied in the high energy physics community, as well [18–20], although the theoretical interpretation of the results is less clear and not well developed. Until now, it has been impossible to quantitatively compare femtosopic results from hadron-hadron collisions to those from heavy ion collisions, due to divergent and often undocumented analysis techniques, detector acceptances and

fitting functions historically used in the high energy community [20].

In this paper, we exploit the unique opportunity offered by the STAR/RHIC experiment, to make the first direct comparison and quantitative connection between femtoscopy in proton-proton and heavy ion collisions. Systematic complications in comparing these collisions are greatly reduced by using an identical detector and reconstruction software, collision energies, and analysis techniques (e.g. event mixing [21], see below). We observe and discuss the importance of non-femtosopic correlations in the analysis of small systems, and put our femtosopic results for $p + p$ collisions into the context both of heavy ion collisions and (as much as possible) of previous high-energy measurements on hadron-hadron and $e^+ + e^-$ collisions. These results may play a role in understanding the physics behind the space-momentum correlations in these collisions, in the same way that comparison of $p + p$ and heavy ion collision results in the high- p_T sector is crucial for understanding the physics of partonic energy loss [1–4, 22]. Our direct comparison also serves as a model and baseline for similar comparisons soon to be possible at higher energies at the Large Hadron Collider.

The paper is organized as follows. In Section II, we discuss the construction of the correlation function and the forms used to parameterize it. Section III discusses details of the analysis, and the results are presented in Section IV. In Section V, we put these results in the context of previous measurements in Au + Au and $p + p(\bar{p})$ collisions. We discuss the similarity between the systematics of HBT radii in heavy ion and particle collisions in Section VI and summarize in Section VII.

II. TWO-PARTICLE CORRELATION FUNCTION

The two-particle correlation function is generally defined as the ratio of the probability of the simultaneous measurement of two particles with momenta p_1 and p_2 , to the product of single-particle probabilities,

$$C(\vec{p}_1, \vec{p}_2) \equiv \frac{P(\vec{p}_1, \vec{p}_2)}{P(\vec{p}_1)P(\vec{p}_2)}. \quad (1)$$

In practice, one usually studies the quantity

$$C_{\bar{P}}(\vec{q}) = \frac{A_{\bar{P}}(\vec{q})}{B_{\bar{P}}(\vec{q})}, \quad (2)$$

where $\vec{q} \equiv \vec{p}_1 - \vec{p}_2$. $A(\vec{q})$ is the distribution of the pairs from the same event, and $B(\vec{q})$ is the reference (or “background”) distribution. B contains all single-particle effects, including detector acceptance and efficiency, and is usually calculated with an event-mixing technique [11, 21]. The explicit label $\bar{P} (\equiv (\vec{p}_1 + \vec{p}_2)/2)$ emphasizes that separate correlation functions are constructed and fitted (see below) as a function of \vec{q} , for different selections of the total momentum \vec{P} ; following convention, we drop the explicit subscript below. Sometimes the measured ratio is normalized to unity at large values of $|\vec{q}|$; we include the normalization in the fit.

In older or statistics-challenged experiments, the correlation function is sometimes constructed in the one-dimensional quantity $Q_{\text{inv}} \equiv \sqrt{(\vec{p}_1 - \vec{p}_2)^2 - (E_1 - E_2)^2}$ or two-dimensional variants (see below). More commonly in recent experiments, it is constructed in three dimensions in the so-called the “out-side-long” coordinate system [23–25]. In this system, the “out” direction is that of the pair transverse momentum, the “long” direction is parallel to the beam, and the “side” direction is orthogonal to these two. We will use the subscripts “o,” “l” and “s” to indicate quantities in these directions.

It has been suggested [26–28] to construct the three-dimensional correlation function using spherical coordinates

$$q_o = |\vec{q}| \sin \theta \cos \phi, \quad q_s = |\vec{q}| \sin \theta \sin \phi, \quad q_l = |\vec{q}| \cos \theta. \quad (3)$$

This aids in making a direct comparison to the spatial separation distribution through imaging techniques and provides an efficient way to visualize the full three-dimensional structure of $C(\vec{q})$. The more traditional “Cartesian projections” in the “o,” “s” and “l” directions integrate over most of the three-dimensional structure, especially at large relative momentum [11, 28].

Below, we will present data in the form of the spherical harmonic decomposition coefficients, which depend explicitly on $|\vec{q}|$ as

$$A_{l,m}(|\vec{q}|) \equiv \frac{1}{\sqrt{4\pi}} \int d\phi d(\cos \theta) C(|\vec{q}|, \theta, \phi) Y_{l,m}(\theta, \phi). \quad (4)$$

The coefficient $A_{00}(|\vec{q}|)$ represents the overall angle-integrated strength of the correlation. $A_{20}(|\vec{q}|)$ and $A_{22}(|\vec{q}|)$ are the quadrupole moments of C at a particular value of $|\vec{q}|$. In particular, A_{22} quantifies the second-order oscillation around the “long” direction; in the simplest HBT analysis, this term reflects non-identical values of the R_o and R_s HBT radii (c.f. below). Coefficients with odd l represent a dipole moment of the correlation function and correspond to a “shift” in the average position of the first particle in a pair, relative to the second [26–28]. In the present case of identical particles, the labels “first” and “second” become meaningless, and odd- l terms vanish by symmetry. Likewise, for the present case, odd- m terms, and all imaginary components vanish as well. See Appendix B of [28] for a full discussion of symmetries.

In heavy ion collisions, it is usually assumed that all of the correlations between identical pions at low relative momentum are due to femtoscopic effects, i.e. quantum statistics and final-state interactions [11]. At large $|\vec{q}|$, femtoscopic effects vanish [e.g. 11]. Thus, in the absence of other correlations, $C(\vec{q})$ must approach a constant value independent of the magnitude and direction of \vec{q} ; equivalently, $A_{l,m}(|\vec{q}|)$ must vanish at large $|\vec{q}|$ for $l \neq 0$.

However, in elementary particle collisions additional structure at large relative momentum ($|\vec{q}| \gtrsim 400$ MeV/c) has been observed [e.g. 20, 29–33]. Usually this structure is parameterized in terms of a function $\Omega(\vec{q})$ that contributes in addition to the femtoscopic component $C_F(\vec{q})$. Explicitly including the normalization parameter \mathcal{N} , then, we will fit our measured

correlation functions with the form

$$C(\vec{q}) = \mathcal{N} \cdot C_F(\vec{q}) \cdot \Omega(\vec{q}). \quad (5)$$

Below, we discuss separately various parameterizations of the femtoscopic and non-femtoscopic components, which we use in order to connect with previous measurements. A historical discussion of these forms may be found in [20].

We use a maximum-likelihood fit to the correlation functions, though chi-square minimization yields almost identical results, and we give the χ^2 values for all fits below. As we shall see, none of the functional forms perfectly fits the data. However, the characteristic scales of the source can be extracted and compared with identical fits to previous data.

A. Femtoscopic correlations

Femtoscopic correlations between identical pions are dominated by Bose-Einstein symmetrization and Coulomb final state effects in the two-pion wavefunction [11].

In all parameterizations, the overall strength of the femtoscopic correlation is characterized by a parameter λ [11]. Historically called the “chaoticity” parameter, it generally accounts for particle identification efficiency, long-lived decays, and long-range tails in the separation distribution [34].

In the simplest case, the Bose-Einstein correlations are often parameterized by a Gaussian,

$$C_F(Q_{\text{inv}}) = 1 + \lambda e^{-Q_{\text{inv}}^2 R_{\text{inv}}^2}, \quad (6)$$

where R_{inv} is a one dimensional “HBT radius.”

Kopylov and Podgoretskii [35] introduced an alternative, two-dimensional parameterization

$$C_F(q_T, q_0) = 1 + \lambda \left[\frac{2J_1(q_T R_B)}{q_T R_B} \right]^2 (1 + q_0^2 \tau^2)^{-1}, \quad (7)$$

where q_T is the component of \vec{q} orthogonal to \vec{P} , $q_0 = E_1 - E_2$, R_B and τ are the size and decay constants of a spherical emitting source, and J_1 is the first order Bessel function. This is similar to another common historical parameterization [e.g. 36] characterizing the source with a spatial and temporal scale

$$C_F(q, q_0) = 1 + \lambda e^{-q_T^2 R_G^2 - q_0^2 \tau^2}. \quad (8)$$

Simple numerical studies show that R_G from Eq. 8 is approximately half as large as R_B obtained from Eq. 7 [20, 36, 37].

With sufficient statistics, a three-dimensional correlation function may be measured. We calculate the relative momentum in the longitudinally co-moving system (LCMS), in which the total longitudinal momentum of the pair, $p_{l,1} + p_{l,2}$, vanishes [38]. For heavy ion and hadron-hadron collisions, this “longitudinal” direction \hat{l} is taken to be the beam axis [11]; for $e^+ + e^-$ collisions, the thrust axis is used.

For a Gaussian emission source, femtoscopic correlations due only to Bose-Einstein symmetrization are given by [e.g. 11]

$$C_F(q_o, q_s, q_l) = 1 + \lambda e^{-q_o^2 R_o^2 - q_s^2 R_s^2 - q_l^2 R_l^2}, \quad (9)$$

where R_o , R_s and R_l are the spatial scales of the source.

While older papers sometimes ignored the Coulomb final state interaction between the charged pions [20], it is usually included by using the Bowler-Sinyukov [39, 40] functional form

$$C_F(Q_{\text{inv}}) = (1 - \lambda) + \lambda K_{\text{Coul}}(Q_{\text{inv}}) \left(1 + e^{-Q_{\text{inv}}^2 R_{\text{inv}}^2}\right), \quad (10)$$

and in 3D,

$$C_F(q_o, q_s, q_l) = (1 - \lambda) + \lambda K_{\text{Coul}}(Q_{\text{inv}}) \times \left(1 + e^{-q_o^2 R_o^2 - q_s^2 R_s^2 - q_l^2 R_l^2}\right). \quad (11)$$

Here, K_{Coul} is the squared Coulomb wavefunction integrated over the source emission points and over the angles of the relative momentum vector in the pair rest frame.

B. Non-femtoscopic correlations

In the absence of non-femtoscopic effects, one of the forms for $C_F(\vec{q})$ from Section II A is fitted to the measured correlation function; i.e. $\Omega = 1$ in Equation 5. Such a “standard fit” works well in the high-multiplicity environment of heavy ion collisions [11]. In hadron-hadron or $e^+ + e^-$ collisions, however, it does not describe the measured correlation function well, especially as $|q|$ increases. Most authors attribute the non-femtoscopic structure to momentum conservation effects in these small systems. While this large- $|q|$ behavior is sometimes simply ignored, it is usually included in the fit either through ad-hoc [30] or physically-motivated [28] terms.

In this paper, we will use three selected parameterizations of the non-femtoscopic correlations and study their effects on the femtoscopic parameters obtained from the fit to experimental correlation functions. The first formula assumes that the non-femtoscopic contribution can be parameterized by a first-order polynomial in \vec{q} -components (used e.g. in [41–45]). Respectively, the one- and three-dimensional forms used in the literature are

$$\Omega(q) = 1 + \delta q \quad (12)$$

and

$$\Omega(\vec{q}) = \Omega(q_o, q_s, q_l) = 1 + \delta_o q_o + \delta_s q_s + \delta_l q_l. \quad (13)$$

For simplicity, we will use the name “ $\delta - q$ fit” when we fit Eq. 12 or 13 to one- or three-dimensional correlation functions.

Another form [46] assumes that non-femtoscopic correlations contribute $|\vec{q}|$ -independent values to the $l = 2$ moments in Equation 4. In terms of the fitting parameters ζ and β ,

$$\begin{aligned} \Omega(|\vec{q}|, \cos \theta, \phi) &= \Omega(\cos \theta, \phi) = \\ &1 + 2\sqrt{\pi}(\beta Y_{2,0}(\cos \theta, \phi) + 2\zeta \text{Re}[Y_{2,2}(\cos \theta, \phi)]) = \\ &1 + \beta \sqrt{\frac{5}{4}}(3 \cos^2 \theta - 1) + \zeta \sqrt{\frac{15}{2}} \sin^2 \theta \cos 2\phi. \end{aligned} \quad (14)$$

For simplicity, fits using this form for the non-femtoscopic effects will be referred to as “ $\zeta - \beta$ fits.”

These two forms (as well as others that can be found in literature [20]) are purely empirical, motivated essentially by the shape of the observed correlation function itself. While most authors attribute these effects primarily to momentum conservation in these low-multiplicity systems, the parameters and functional forms themselves cannot be directly connected to this or any physical mechanism. One may identify two dangers of using an ad-hoc form to quantify non-femtoscopic contributions to $C(\vec{q})$. Firstly, while they describe (by construction) the correlation function well at large $|\vec{q}|$, for which femtoscopic contributions vanish, there is no way to constrain their behaviour at low $|\vec{q}|$ where both femtoscopic and (presumably) non-femtoscopic correlations exist. Even simple effects like momentum conservation give rise to non-femtoscopic correlations that vary non-trivially even at low $|\vec{q}|$. Misrepresenting the non-femtoscopic contribution in $\Omega(\vec{q})$ can therefore distort the femtoscopic radius parameters in $C_F(\vec{q})$, especially considering the small radius values in $p + p$ collisions. Secondly, there is no way to estimate whether the best-fit parameter values in an ad-hoc functional form are physically “reasonable.”

If the non-femtoscopic correlations are in fact dominated by energy and momentum conservation, as is usually supposed, one may derive an analytic functional form for Ω . In particular, the multiparticle phase space constraints for a system of N particles project onto the two-particle space as [28]

$$\begin{aligned} \Omega(p_1, p_2) &= 1 - M_1 \cdot \overline{\{\vec{p}_{1,T} \cdot \vec{p}_{2,T}\}} - M_2 \cdot \overline{\{p_{1,z} \cdot p_{2,z}\}} \\ &\quad - M_3 \cdot \overline{\{E_1 \cdot E_2\}} + M_4 \cdot \overline{\{E_1 + E_2\}} - \frac{M_4^2}{M_3}, \end{aligned} \quad (15)$$

where

$$\begin{aligned} M_1 &\equiv \frac{2}{N \langle p_T^2 \rangle}, & M_2 &\equiv \frac{1}{N \langle p_z^2 \rangle} \\ M_3 &\equiv \frac{1}{N (\langle E^2 \rangle - \langle E \rangle^2)}, & M_4 &\equiv \frac{\langle E \rangle}{N (\langle E^2 \rangle - \langle E \rangle^2)}. \end{aligned} \quad (16)$$

The notation $\overline{\{X\}}$ in Equation 15 is used to indicate that X is the average of a two-particle quantity which depends on p_1 and p_2 (or \vec{q} , etc). In particular,

$$\overline{\{X\}}(\vec{q}) \equiv \frac{\int d^3 \vec{p}_1 \int d^3 \vec{p}_2 P(\vec{p}_1) P(\vec{p}_2) X \delta(\vec{q} - (\vec{p}_1 - \vec{p}_2))}{\int d^3 \vec{p}_1 \int d^3 \vec{p}_2 P(\vec{p}_1) P(\vec{p}_2) \delta(\vec{q} - (\vec{p}_1 - \vec{p}_2))}, \quad (17)$$

where P represents the single-particle probability first seen in Equation 1.

In practice, this means generating histograms in addition to $A(\vec{q})$ and $B(\vec{q})$ (c.f. Equation 2) as one loops over mixed pairs of particles i and j in the data analysis. For example

$$\overline{\{\vec{p}_{1,T} \cdot \vec{p}_{2,T}\}}(\vec{q}) = \frac{(\sum_{i,j} \vec{p}_{i,T} \cdot \vec{p}_{j,T})(\vec{q})}{B(\vec{q})}, \quad (18)$$

where the sum in the numerator runs over all pairs in all events.

In Equation 15, the four fit parameters M_i are directly related to five physical quantities, (N - the number of particles, $\langle p_T^2 \rangle$, $\langle p_z^2 \rangle$, $\langle E^2 \rangle$, $\langle E \rangle$) through Eq. 16. Assuming that

$$\langle E^2 \rangle \approx \langle p_T^2 \rangle + \langle p_z^2 \rangle + m_*^2, \quad (19)$$

where m_* is the mass of a typical particle in the system (for our pion-dominated system, $m_* \approx m_\pi$), then one may solve for the physical parameters. For example,

$$N \approx \frac{M_1^{-1} + M_2^{-1} - M_3^{-1}}{\left(\frac{M_4}{M_3}\right)^2 - m_*^2}. \quad (20)$$

Since we cannot know exactly the values of $\langle E^2 \rangle$ etc, that characterize the underlying distribution in these collisions, we treat the M_i as free parameters in our fits, and then consider whether their values are mutually compatible and physical. For a more complete discussion, see [28, 47].

In [28], the correlations leading to Equation 15 were called ‘‘EMCICs’’ (short for Energy and Momentum Conservation-Induced Correlations); we will refer to fits using this function with this acronym, in our figures.

C. Parameter counting

As mentioned, we will be employing a number of different fitting functions, each of which contains several parameters. It is appropriate at this point to briefly take stock.

In essentially all modern HBT analyses, on the order of 5-6 parameters quantify the femtoscopic correlations. For the common Gaussian fit (equation 11), one has three ‘‘HBT radii,’’ the chaoticity parameter, and the normalization \mathcal{N} . Recent ‘‘imaging’’ fits approximate the two-particle emission zone as a sum of spline functions, the weights of which are the parameters [48]; the number of splines (hence weights) used is ~ 5 . Other fits (e.g. double Gaussian, exponential-plus-Gaussian) [18, 49] contain a similar number of femtoscopic parameters. In all cases, a distinct set of parameters is extracted for each selection of \vec{P} (c.f. equation 2 and surrounding discussion).

Accounting for the non-femtoscopic correlations inevitably increases the total number of fit parameters. The ‘‘ $\zeta - \beta$ ’’ functional form (eq. 14) involves two parameters, the ‘‘ $\delta - q$ ’’ form (eq. 13) three, and the EMCIC form (eq. 15) four. However, it is important to keep in mind that using the $\zeta - \beta$ ($\delta - q$) form means 2 (3) additional parameters for each selection of \vec{P} when forming the correlation functions. On the other hand, the four EMCICs parameters cannot depend on \vec{P} . Therefore, when fitting $C_{\vec{P}}(\vec{q})$ for four selections of \vec{P} , use of the $\zeta - \beta$, $\delta - q$ and EMCIC forms increases the total number of parameters by 8, 12 and 4, respectively.

III. ANALYSIS DETAILS

As mentioned in Section I, there is significant advantage in analyzing $p + p$ collisions in the same way that heavy ion

collisions are analyzed. Therefore, the results discussed in this paper are produced with the same techniques and acceptance cuts as have been used for previous pion femtoscopy studies by STAR [50–53]. Here we discuss some of the main points; full systematic studies of cuts and techniques can be found in [52].

The primary sub-detector used in this analysis to reconstruct particles is the Time Projection Chamber (TPC) [54]. Pions could be identified up to a momentum of 800 MeV/c by correlating their momentum and specific ionization loss (dE/dx) in the TPC gas. A particle was considered to be a pion if its dE/dx value for a given momentum was within two sigma of the Bichsel expectation [55] (an improvement on the Bethe-Bloch formula [56] for thin materials) for a pion, and more than two sigma from the expectations for electrons, kaons and protons. By varying the cuts on energy loss to allow more or less contamination from kaons or electrons, we estimate that impurities in the pion sample lead to an uncertainty in the femtoscopic scale parameters (e.g. HBT radii) of only about 1%. Particles were considered for analysis if their reconstructed tracks produced hits on at least 10 of the 45 padrows, and their distance of closest approach (DCA) to the primary vertex was less than 3 cm. The lower momentum cut of 120 MeV/c is imposed by the TPC acceptance and the magnetic field. Only tracks at midrapidity ($|y| < 0.5$) were included in the femtoscopic analysis.

Events were recorded based on a coincidence trigger of two Beam-Beam Counters (BBCs), annular scintillator detectors located ± 3.5 m from the interaction region and covering pseudorapidity range $3.3 < |\eta| < 5.0$. Events were selected for analysis if the primary collision vertex was within 30 cm of the center of the TPC. The further requirement that events include at least two like-sign pions increases the average charged particle multiplicity with $|\eta| < 0.5$ from 3.0 (without the requirement) to 4.25. Since particle pairs enter into the correlation function, the effective average multiplicity is higher; in particular, the pair-weighted charged-particle multiplicity at midrapidity is about 6.0. After event cuts, about 5 million minimum bias events from $p + p$ collisions at $\sqrt{s} = 200$ GeV were used.

Two-track effects, such as splitting (one particle reconstructed as two tracks) and merging (two particles reconstructed as one track) were treated identically as has been done in STAR analyses of Au + Au collisions [52]. Both effects can affect the shape of $C(\vec{q})$ at very low $|\vec{q}| \lesssim 20$ MeV/c, regardless of the colliding system. However, their effect on the extracted sizes in $p + p$ collisions turns out to be smaller than statistical errors, due to the fact that small (~ 1 fm) sources lead to large (~ 200 MeV/c) femtoscopic structures in the correlation function.

The analysis presented in this paper was done for four bins in average transverse momentum k_T ($\equiv \frac{1}{2} |(\vec{p}_{T,1} + \vec{p}_{T,2})|$): 150-250, 250-350, 350-450 and 450-600 MeV/c. The systematic errors on femtoscopic radii due to the fit range, particle mis-identification, two-track effects and the Coulomb radius (used to calculate K_{coul} in Eqs. 10 and 11) are estimated to be about 10%, similar to previous studies [52].

IV. RESULTS

In this section, we present the correlation functions and fits to them, using the various functional forms discussed in Section II. The m_T and multiplicity dependence of femtoscopic radii from these fits are compared here, and put into the broader context of data from heavy ion and particle collisions in the next section.

Figure 1 shows the two-pion correlation function for minimum-bias $p + p$ collisions for $0.35 < k_T < 0.45$ GeV/c. The three-dimensional data is represented with the traditional one-dimensional Cartesian projections [11]. For the projection on q_o , integration in q_s and q_l was done over the range $[0.00, 0.12]$ GeV/c. As discussed in Section II and in more detail in [28], the full structure of the correlation function is best seen in the spherical harmonic decomposition, shown in Figs. 2-5.

In what follows, we discuss systematics of fits to the correlation function, with particular attention to the femtoscopic parameters. It is important to keep in mind that the fits are performed on the full three-dimensional correlation function $C(\vec{q})$. The choice to plot the data and fits as spherical harmonic coefficients A_{lm} or as Cartesian projections along the “out,” “side” and “long” directions is based on the desire to present results in the traditional format (projections) or in a representation more sensitive to the three-dimensional structure of the data [28]. In particular, the data and fits shown in Fig. 1, for $k_T=0.35-0.45$ GeV/c, are the same as those shown in Fig. 4.

A. Transverse mass dependence of 3D femtoscopic radii

Femtoscopic scales from three-dimensional correlation functions are usually extracted by fitting to the functional form given in Equation 11. In order to make connection to previous measurements, we employ the same form and vary the treatment of non-femtoscopic effects as discussed in Section II B. The fits are shown as curves in Fig. 1-5; the slightly fluctuating structure observable in the sensitive spherical harmonic representation in Fig. 2-5 results from finite-binning effects in plotting [57].

Dashed green curves in Figs. 1-5 represent the “standard fit,” in which non-femtoscopic correlations are neglected altogether ($\Omega = 1$). Black dotted and purple dashed curves, respectively, indicate “ $\delta - q$ ” (Equation 13) and “ $\zeta - \beta$ ” (Equation 14) forms. Solid red curves represent fits in which the non-femtoscopic contributions follow the EMCIC (Equation 15) form. None of the functional forms perfectly fits the experimental correlation function, though the non-femtoscopic structure is semi-quantitatively reproduced by the ad-hoc $\delta - q$ and $\zeta - \beta$ fits (by construction) and the EMCIC fit (non-trivially). Rather than invent yet another ad-hoc functional form to better fit the data, we will consider the radii produced by all of these forms.

The fit parameters for these four fits, for each of the four k_T bins, are given in Tables I-IV. Considering first the non-femtoscopic correlations, we observe that the ad-hoc fit parameters $\delta_{O,S,L}$ and ζ and β in Tables III and II are different

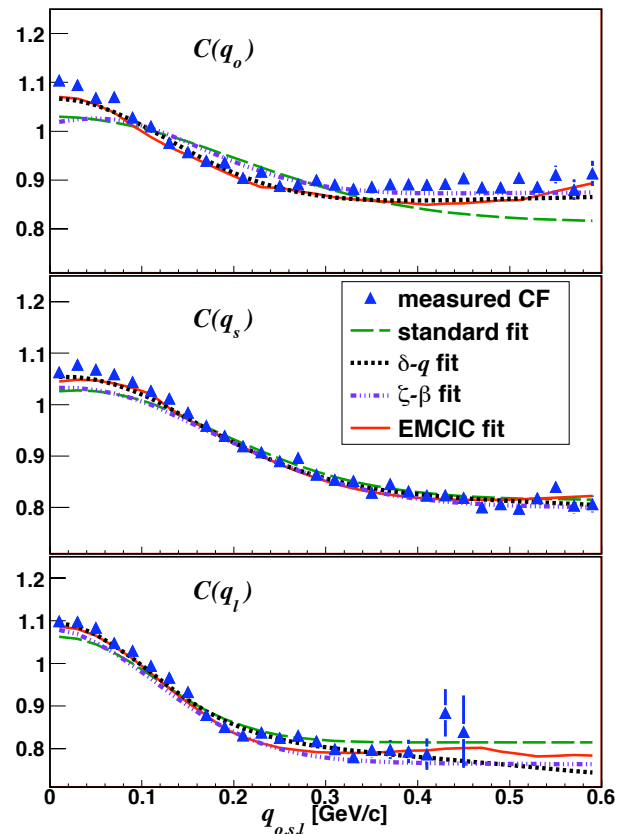


FIG. 1: (Color online) Cartesian projections of the 3D correlation function from $p + p$ collisions at $\sqrt{s}=200$ GeV for $k_T = [0.35, 0.45]$ GeV/c (blue triangles). Femtoscopic effects are parameterized with the form in Eq. 11; different curves represent various parameterizations of non-femtoscopic correlations used in the fit and described in detail in Sec. II B.

for each k_T bin. Due to their physical meaning, the EMCIC parameters M_{1-4} are fixed for all k_T values, as indicated in Table IV. Setting the characteristic particle mass to that of the pion and using Equations 16, 19 and 20, the non-femtoscopic parameters listed in Table IV correspond to the following values characteristic of the emitting system:

$$\begin{aligned} N &= 14.3 \pm 4.7 \\ \langle p_T^2 \rangle &= 0.17 \pm 0.06 \text{ (GeV/c)}^2 \\ \langle p_z^2 \rangle &= 0.32 \pm 0.13 \text{ (GeV/c)}^2 \\ \langle E^2 \rangle &= 0.51 \pm 0.11 \text{ GeV}^2 \\ \langle E \rangle &= 0.68 \pm 0.08 \text{ GeV.} \end{aligned}$$

These values are rather reasonable [47].

HBT radii from the different fits are plotted as a function of transverse mass in Fig. 6. The treatment of the non-femtoscopic correlations significantly affects the magnitude of the femtoscopic length scales extracted from the fit, especially in the “out” and “long” directions, for which variations up to 50% in magnitude are observed. The dependence of the radii on $m_T \equiv \sqrt{k_T^2 + m^2}$ is quite similar in all cases. We

k_T [GeV/c]	R_o [fm]	R_s [fm]	R_l [fm]	λ	χ^2/ndf
[0.15, 0.25]	0.84 ± 0.02	0.89 ± 0.01	1.53 ± 0.02	0.422 ± 0.004	2012 / 85
[0.25, 0.35]	0.81 ± 0.02	0.88 ± 0.01	1.45 ± 0.02	0.422 ± 0.005	1852 / 85
[0.35, 0.45]	0.71 ± 0.02	0.82 ± 0.02	1.31 ± 0.02	0.433 ± 0.007	941 / 85
[0.45, 0.60]	0.68 ± 0.02	0.68 ± 0.01	1.05 ± 0.02	0.515 ± 0.009	278 / 85

TABLE I: Fit results from a fit to data from $p + p$ collisions at $\sqrt{s} = 200$ GeV using Eq. 11 to parameterize the femtoscopic correlations (“standard fit”).

k_T [GeV/c]	R_o [fm]	R_s [fm]	R_l [fm]	λ	δ_o	δ_s	δ_l	χ^2/ndf
[0.15, 0.25]	1.30 ± 0.03	1.05 ± 0.03	1.92 ± 0.05	0.295 ± 0.004	0.0027 ± 0.0026	-0.1673 ± 0.0052	-0.2327 ± 0.0078	471 / 82
[0.25, 0.35]	1.21 ± 0.03	1.05 ± 0.03	1.67 ± 0.05	0.381 ± 0.005	0.0201 ± 0.0054	-0.1422 ± 0.0051	-0.2949 ± 0.0081	261 / 82
[0.35, 0.45]	1.10 ± 0.03	0.94 ± 0.03	1.37 ± 0.05	0.433 ± 0.007	0.0457 ± 0.0059	-0.0902 ± 0.0053	-0.2273 ± 0.0090	251 / 82
[0.45, 0.60]	0.93 ± 0.03	0.82 ± 0.03	1.17 ± 0.05	0.480 ± 0.009	0.0404 ± 0.0085	-0.0476 ± 0.0093	-0.1469 ± 0.0104	189 / 82

TABLE II: Fit results from a fit to data from $p + p$ collisions at $\sqrt{s} = 200$ GeV using Eq. 11 to parameterize the femtoscopic correlations and Eq. 13 for non-femtoscopic ones (“ $\delta - q$ fit”).

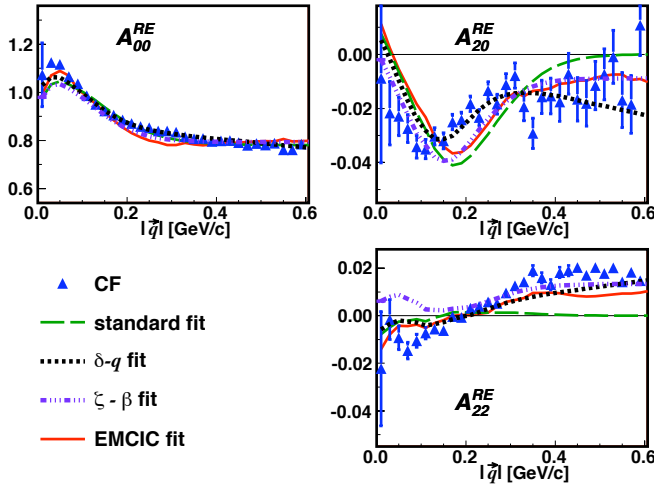


FIG. 2: (Color online) The first three non-vanishing moments of the spherical harmonic decomposition of the correlation function from $p + p$ collisions at $\sqrt{s} = 200$ GeV, for $k_T = [0.15, 0.25]$ GeV/c. Femtoscopic effects are parameterized with the form in Eq. 11; different curves represent various parameterizations of non-femtoscopic correlations used in the fit and described in detail in Sec. II B.

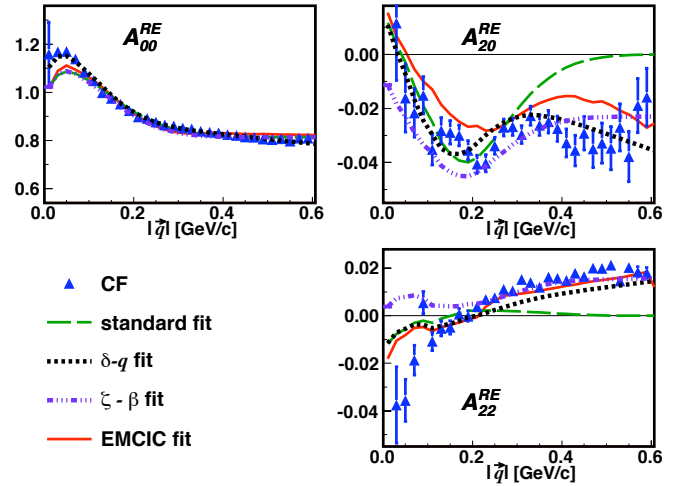


FIG. 3: (Color online) As for Fig. 2, but for $k_T = [0.25, 0.35]$ GeV/c.

discuss this dependence further in Section V.

B. Transverse mass and multiplicity dependence of 1D femtoscopic radii

Since three-dimensional correlation functions encode more information about the homogeneity region than do one-dimensional correlation functions, they are also more statistics hungry. Therefore, most previous particle physics experiments have constructed and analyzed the latter. For the sake of making the connection between our results and existing world systematics, we perform similar analyses as those found in the literature.

The first important connection to make is for the m_T -dependence of HBT radii from minimum-bias $p + p$ collisions. We extract the one-dimensional HBT radius R_{inv} associated with the femtoscopic form in Equation 10, using three forms for the non-femtoscopic terms. For four selections in k_T , Table V lists the fit parameters for the “standard” fit that neglects non-femtoscopic correlations altogether ($\Omega = 1$). Tables VI and VII list results when using the 1-dimensional $\delta - q$ form (Equation 12) and the EMCIC form (Equation 15), respectively. In performing the EMCICs fit, the non-femtoscopic parameters M_{1-4} were kept fixed at the values listed in Table IV.

The one-dimensional radii from the three different treatments of non-femtoscopic effects are plotted as a function of m_T in Fig. 7. The magnitude of the radius using the ad-hoc $\delta - q$ fit is $\sim 25\%$ larger than that from either the standard or EMCIC fit, but again all show similar dependence on m_T .

In order to compare with the multiplicity dependence of

k_T [GeV/c]	R_o [fm]	R_s [fm]	R_l [fm]	λ	ζ	β	χ^2/ndf
[0.15, 0.25]	1.24 ± 0.04	0.92 ± 0.03	1.71 ± 0.04	0.392 ± 0.008	0.0169 ± 0.0021	-0.0113 ± 0.0019	1720 / 83
[0.25, 0.35]	1.14 ± 0.05	0.89 ± 0.04	1.37 ± 0.08	0.378 ± 0.006	0.0193 ± 0.0034	-0.0284 ± 0.0031	823 / 83
[0.35, 0.45]	1.02 ± 0.04	0.81 ± 0.05	1.20 ± 0.07	0.434 ± 0.008	0.0178 ± 0.0029	-0.0289 ± 0.0032	313 / 83
[0.45, 0.60]	0.89 ± 0.04	0.71 ± 0.05	1.09 ± 0.06	0.492 ± 0.009	0.0114 ± 0.0023	-0.0301 ± 0.0041	190 / 83

TABLE III: Fit results from a fit to data from $p + p$ collisions at $\sqrt{s} = 200$ GeV using Eq. 11 to parameterize the femtoscopic correlations and Eq. 14 for non-femtoscopic ones (“ $\zeta - \beta$ fit”).

k_T [GeV/c]	R_o [fm]	R_s [fm]	R_l [fm]	λ	M_1 (GeV/c) $^{-2}$	M_2 (GeV/c) $^{-2}$	M_3 GeV $^{-2}$	M_4 GeV $^{-1}$	χ^2/ndf
[0.15, 0.25]	1.06 ± 0.03	1.00 ± 0.04	1.38 ± 0.05	0.665 ± 0.000	0.43 ± 0.07	0.22 ± 0.06	1.51 ± 0.12	1.02 ± 0.09	2218 / 336
[0.25, 0.35]	0.96 ± 0.02	0.95 ± 0.03	1.21 ± 0.03	0.588 ± 0.006					
[0.35, 0.45]	0.89 ± 0.02	0.88 ± 0.02	1.08 ± 0.04	0.579 ± 0.009					
[0.45, 0.60]	0.78 ± 0.04	0.79 ± 0.02	0.94 ± 0.03	0.671 ± 0.028					

TABLE IV: Fit results from a fit to data from $p + p$ collisions at $\sqrt{s} = 200$ GeV using Eq. 11 to parameterize the femtoscopic correlations and Eq. 15 for non-femtoscopic ones (“EMCIC fit”).

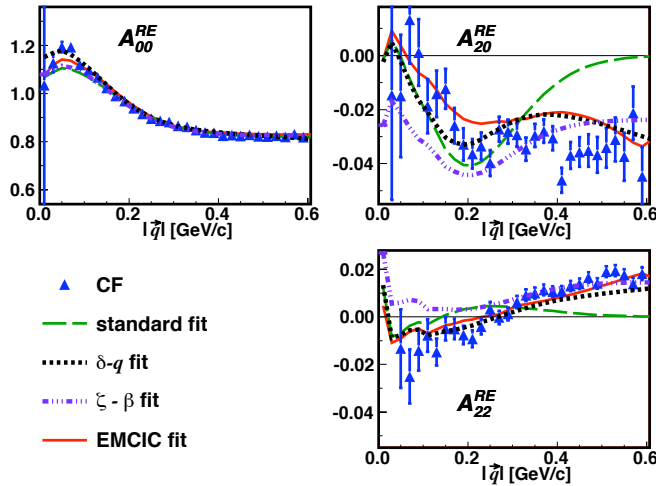


FIG. 4: (Color online) A_s for Fig. 2, but for $k_T = [0.35, 0.45]$ GeV/c.

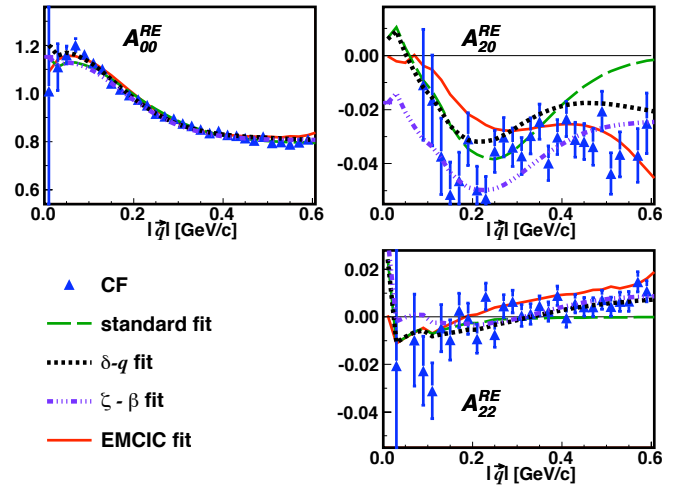


FIG. 5: (Color online) A_s for Fig. 2, but for $k_T = [0.45, 0.60]$ GeV/c.

k_T [GeV/c]	R_{inv} [fm]	λ	χ^2/ndf
[0.15, 0.25]	1.32 ± 0.02	0.345 ± 0.005	265 / 27
[0.25, 0.35]	1.26 ± 0.02	0.357 ± 0.007	203 / 27
[0.35, 0.45]	1.18 ± 0.02	0.348 ± 0.008	243 / 27
[0.45, 0.60]	1.05 ± 0.03	0.413 ± 0.012	222 / 27

TABLE V: Fit results from a fit to 1D correlation function from $p + p$ collisions at $\sqrt{s} = 200$ GeV using Eq. 6 to parameterize the femtoscopic correlations (“standard fit”).

k_T [GeV/c]	R_{inv} [fm]	λ	δ	χ^2/ndf
[0.15, 0.25]	1.72 ± 0.04	0.285 ± 0.007	0.237 ± 0.007	86 / 26
[0.25, 0.35]	1.65 ± 0.04	0.339 ± 0.009	0.163 ± 0.008	80 / 26
[0.35, 0.45]	1.49 ± 0.05	0.308 ± 0.011	0.180 ± 0.015	71 / 26
[0.45, 0.60]	1.41 ± 0.06	0.338 ± 0.016	0.228 ± 0.017	78 / 26

TABLE VI: Fit results from a fit to 1D correlation function from $p + p$ collisions at $\sqrt{s} = 200$ GeV using Eq. 6 to parameterize the femtoscopic correlations and Eq. 12 for non-femtoscopic ones (“ $\delta - q$ fit”).

585 k_T -integrated HBT radii reported in high energy particle col-
 586 lisions, we combine k_T bins and separately analyze low⁵⁹²
 587 ($dN_{ch}/d\eta \leq 6$) and high ($dN_{ch}/d\eta \geq 7$) multiplicity events.⁵⁹³
 588 The choice of the cut was dictated by the requirement of suf-⁵⁹⁴
 589 ficient pair statistics in the two event classes. Fit parame-⁵⁹⁵
 590 ters for common fitting functions are given in Table VIII, for⁵⁹⁶
 591 minimum-bias and multiplicity-selected collisions.⁵⁹⁷

Figure 8 shows the multiplicity dependence of the common one-dimensional HBT radius R_{inv} , extracted by parameterizing the femtoscopic correlations according to Equation 10. Non-femtoscopic effects were either ignored (“standard fit” $\Omega = 1$) or parameterized with the “ $\delta - q$ ” (Eq. 12) or EMCIC (Eq. 15) functional form. In order to keep the parame-

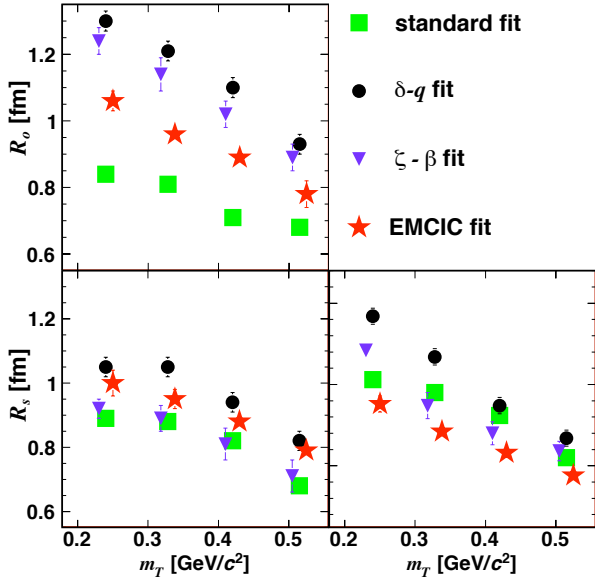


FIG. 6: (Color online) The m_T -dependence of the 3D femtoscopic radii in $p + p$ collisions at $\sqrt{s} = 200$ GeV for different parameterizations of the non-femtoscopic correlations. See text for more details. Data have been shifted slightly in the abscissa, for clarity.

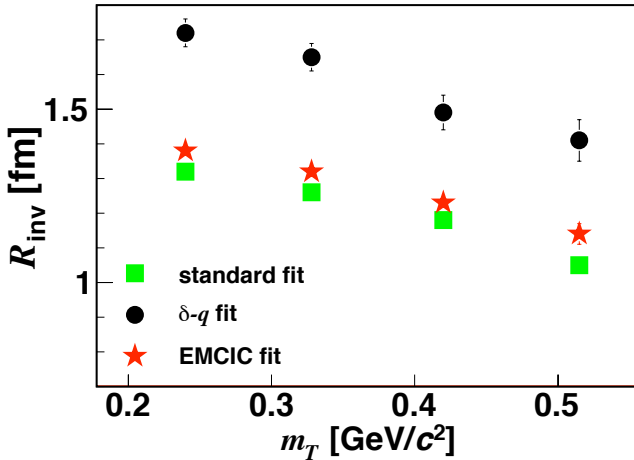


FIG. 7: (Color online) The m_T -dependence of R_{inv} from $p + p$ collisions at $\sqrt{s} = 200$ GeV for different parameterizations of the non-femtoscopic correlations used in the fit procedure.

k_T [GeV/c]	R_{inv} [fm]	λ	χ^2/ndf
[0.15, 0.25]	1.38 ± 0.03	0.347 ± 0.005	99 / 27
[0.25, 0.35]	1.32 ± 0.03	0.354 ± 0.006	97 / 27
[0.35, 0.45]	1.23 ± 0.04	0.349 ± 0.009	86 / 27
[0.45, 0.60]	1.14 ± 0.05	0.411 ± 0.013	80 / 27

TABLE VII: Fit results from a fit to 1D correlation function from $p + p$ collisions at $\sqrt{s} = 200$ GeV using Eq. 6 to parameterize the femtoscopic correlations and Eq. 15 for non-femtoscopic ones (“EMCICs fit”). The non-femtoscopic parameters M_{1-4} were not varied, but kept fixed to the values in Table IV.

point we focus on is that the systematic dependences of the femtoscopic scales, both with k_T and multiplicity, are robust.

Table IX lists fit parameters to two-dimensional correlation functions in q_T and q_0 , using Equations 8 and 7. The radius from the former fit is approximately twice that of the latter, as expected (c.f. Sec. II A). These values will be compared with previously measured data in the next section.

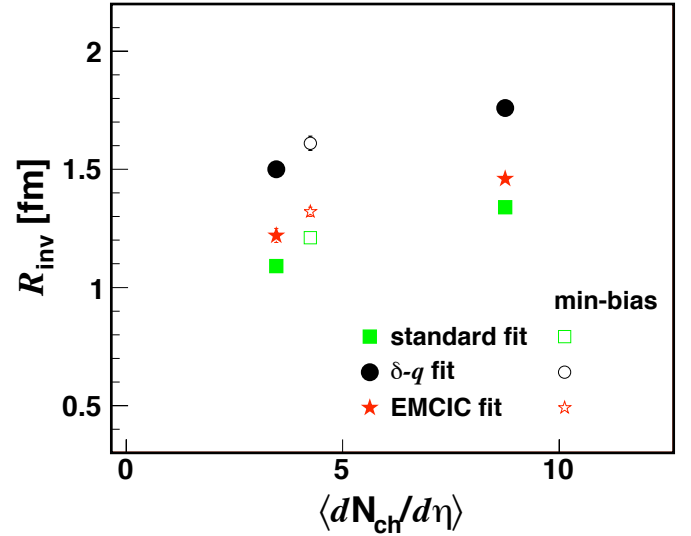


FIG. 8: (Color online) The multiplicity dependence of R_{inv} from $p + p$ collisions at $\sqrt{s} = 200$ GeV for different parameterizations of the non-femtoscopic correlations. Pions within the range of $k_T = [0.15, 0.60]$ GeV/c were used in the analysis.

598 ter count down, the EMCIC, the kinematic parameters ($\langle p_T^2 \rangle$,
 599 $\langle p_z^2 \rangle$, $\langle E^2 \rangle$, $\langle E \rangle$) were kept fixed to the values obtained from
 600 the 3-dimensional fit, and only N was allowed to vary. In all
 601 cases, R_{inv} is observed to increase with multiplicity. Param-
 602 eterizing non-femtoscopic effects according to the EMCIC
 603 form gives similar results as a “standard” fit ignoring them,
 604 whereas the “ $\delta - q$ ” form generates an offset of approximately
 605 0.3 fm offset, similar to all three- and one-dimensional fits
 606 discussed above. That different numerical values are obtained
 607 for somewhat different fitting functions, is not surprising. The

V. COMPARISON WITH WORLD SYSTEMATICS

In this section, we make the connection between femtoscopic measurements in heavy ion collisions and those in particle physics, by placing our results in the context of world systematics from each.

method	fit parameter	$\langle dN_{ch}/d\eta \rangle$		
		4.25 (min-bias)	3.47	8.75
standard fit	R_{inv}	1.21 ± 0.01	1.09 ± 0.02	1.34 ± 0.02
	λ	0.353 ± 0.003	0.347 ± 0.04	0.356 ± 0.03
	χ^2/ndf	202 / 27	100 / 27	92 / 27
$\delta - q$ fit	R_{inv}	1.61 ± 0.01	1.50 ± 0.03	1.76 ± 0.03
	λ	0.312 ± 0.003	0.275 ± 0.005	0.322 ± 0.007
	δQ_{inv}	-0.191 ± 0.003	-0.242 ± 0.005	-0.194 ± 0.006
	χ^2/ndf	159 / 26	83 / 26	73 / 26
EMCIC fit	R_{inv}	1.32 ± 0.02	1.22 ± 0.03	1.46 ± 0.02
	λ	0.481 ± 0.003	0.485 ± 0.003	0.504 ± 0.004
	N	14.3 ± 4.7	11.8 ± 7.1	26.3 ± 8.4
	χ^2/ndf	161 / 26	80 / 26	75 / 26

TABLE VIII: Multiplicity dependence of fit results to 1D correlation function from $p + p$ collisions at $\sqrt{s} = 200$ GeV for different fit parameterizations.

method	fit parameter	$\langle dN_{ch}/d\eta \rangle$		
		4.25 (min-bias)	3.47	8.75
Eq. 7	R_B	1.79 ± 0.01	1.61 ± 0.02	1.92 ± 0.02
	τ	1.03 ± 0.02	0.98 ± 0.02	1.24 ± 0.03
	λ	0.353 ± 0.003	0.354 ± 0.003	0.334 ± 0.004
	χ^2/ndf	5308 / 896	2852 / 896	1890 / 896
Eq. 8	R_G	1.01 ± 0.01	0.89 ± 0.01	1.07 ± 0.01
	τ	0.76 ± 0.01	0.73 ± 0.02	0.91 ± 0.02
	λ	0.353 ± 0.003	0.352 ± 0.003	0.332 ± 0.004
	χ^2/ndf	5749 / 896	3040 / 896	2476 / 896

TABLE IX: Multiplicity dependence of fit parameters to two-dimensional correlation functions from $p + p$ collisions at $\sqrt{s} = 200$ GeV using Equations 7 and 8. To consistently compare to previous measurements, Ω was set to unity (c.f. Equation 5).

A. Results in the Context of Heavy Ion Systematics

The present measurements represent the first opportunity to study femtoscopic correlations from hadronic collisions and heavy ion collisions, using the same detector, reconstruction, analysis and fitting techniques. The comparison should be direct, and differences in the extracted HBT radii should arise from differences in the source geometry itself. In fact, especially in recent years, the heavy ion community has generally arrived at a consensus among the different experiments, as far as analysis techniques, fitting functions and reference frames to use. This, together with good documentation of event selection and acceptance cuts, has led to a quantitatively consistent world systematics of femtoscopic measurements in heavy ion collisions over two orders of magnitude in collision energy [11]; indeed, at RHIC, the agreement in HBT radii from the different experiments is remarkably good. Thus, inasmuch as STAR’s measurement of HBT radii from $p + p$ collisions may be directly compared with STAR’s HBT radii from Au + Au collisions, they may be equally well compared to the world’s systematics of all heavy ion collisions.

As with most heavy ion observables at low transverse momentum [58], the HBT radii R_s and R_l scale primarily with

event multiplicity [11] (or, at lower energies, with the number of particles of different species [59, 60]) rather than energy or impact parameter. The radius R_o , which nontrivially combines space and time, shows a less clear scaling [11], retaining some energy dependence. As seen in Fig. 9, the radii from $p + p$ collisions at $\sqrt{s} = 200$ GeV fall naturally in line with this multiplicity scaling. On the scale relevant for this comparison, the specific treatment of non-femtoscopic correlations is unimportant.

One of the most important systematics in heavy ion femtoscopy is the m_T -dependence of HBT radii, which directly measures space-momentum correlations in the emitting source at freeze-out; in these large systems, the m_T -dependence is often attributed to collective flow [6]. As we saw in Fig. 6, a significant dependence is seen also for $p + p$ collisions. Several authors [e.g. 18, 30, 31, 36, 61] have remarked on the qualitative “similarity” of the m_T -dependence of HBT radii measured in high energy particle collisions, but the first direct comparison is shown in Fig. 10. There, the ratios of the three dimensional radii in Au + Au collisions to $p + p$ radii obtained with different treatments of the non-femtoscopic correlations, are plotted versus m_T . Well beyond qualitative similarity, the ratios are remarkably flat—i.e.

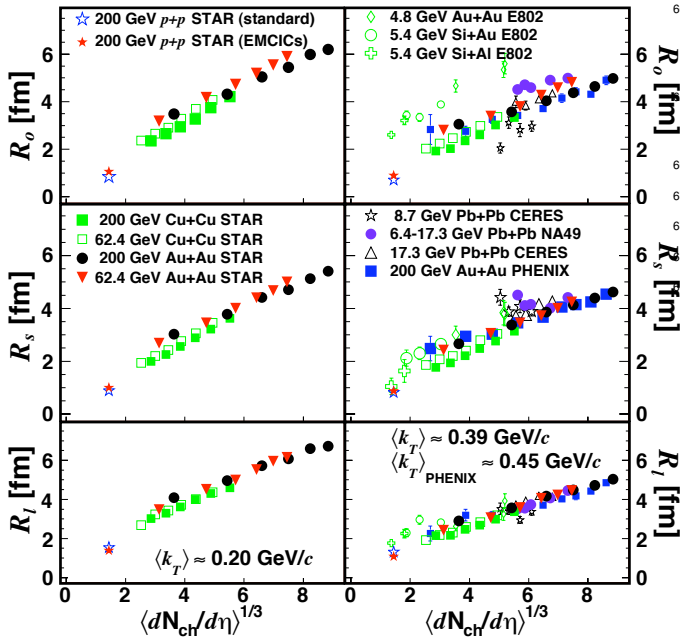


FIG. 9: (Color online) The multiplicity dependence of the HBT radii from $p+p$, Cu+Cu [53] and Au+Au [52, 53] collisions from STAR compared with results from other experiments [11]. Left and right panels show radii measured with $\langle k_T \rangle \approx 0.2$ and 0.39 GeV/ c , respectively. Radii from $p+p$ collisions are shown by blue (“standard fit”) and red (“EMCIC fit”) stars.

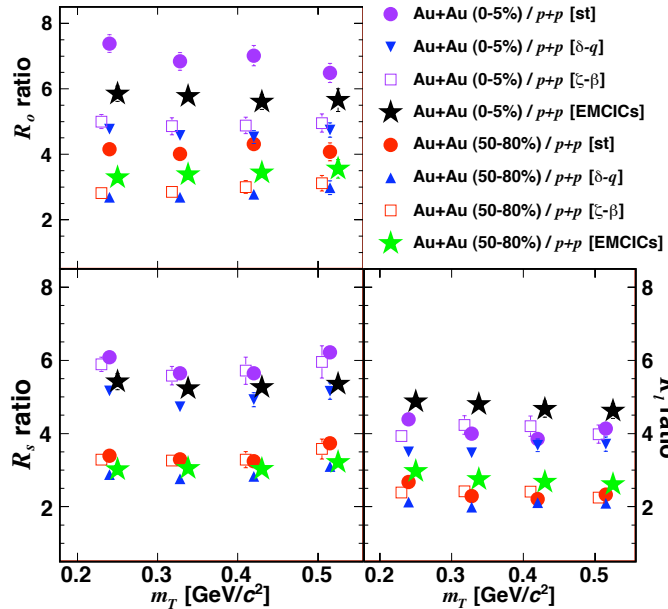


FIG. 10: (Color online) The ratio of the HBT radii from Au+Au collisions [52] to results from $p+p$ collisions plotted versus the transverse mass.

on the possible meaning of this in Section V B.

B. Results in the context of high-energy particle measurements

Recently, a review of the femtoscopic results [20] from particle collisions like $p+p$, $p+\bar{p}$ and $e^+ + e^-$ studied at different energies has been published. Here, we compare STAR results from $p+p$ collisions at $\sqrt{s} = 200$ GeV with world systematics.

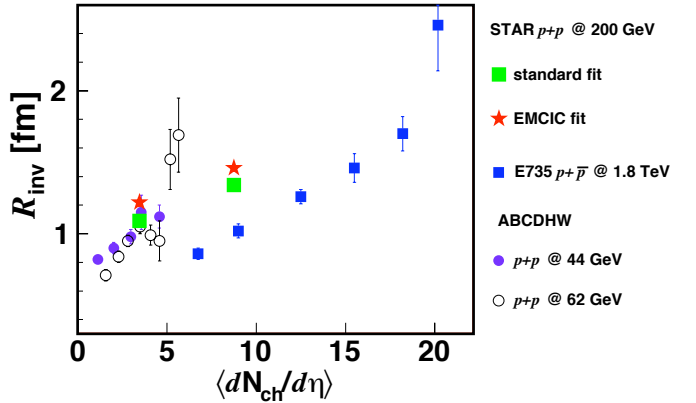


FIG. 11: (Color online) The multiplicity dependence of the 1D femtoscopic radius R_{inv} from hadronic collisions measured by STAR, E735 [36], and ABCDHW [62] collaborations.

The multiplicity dependence of femtoscopic parameters from one- and two-dimensional correlation functions are shown in Figs. 11 and 12. For any given experiment, the radius parameter increases with event multiplicity. However, in contrast to the nearly “universal” multiplicity dependence seen in heavy ion collisions (c.f. Fig. 9), only a qualitative trend is observed, when the different measurements are compared.

There are several possible reasons for this lack or “universality” [20]. Clearly one possibility is that there is no universal multiplicity dependence of the femtoscopic scales; the underlying physics driving the space-time freezeout geometry may be quite different, considering \sqrt{s} varies from 44 to 1800 GeV in the plot. However, even if there were an underlying universality between these systems, it is not at all clear that it would appear in this figure, due to various difficulties in tabulating historical data [20]. Firstly, as discussed in Section II the experiments used different fitting functions to extract the HBT radii, making direct comparison between them difficult. Secondly, as we have shown, the radii depend on both multiplicity and k_T . Since, for statistical reasons, the results in Fig. 9 are integrated over the acceptance of each experiment, and these acceptances differ strongly, any universal scaling would be obscured. For example, since the acceptance of Tevatron experiment E735 [36] is weighted towards higher k_T than the other measurements, one expects a systematically lower HBT radius, at a given multiplicity. Indeed, even the “universal” multiplicity scaling in heavy ion collisions is only universal

665 the m_T -dependence in $p+p$ collisions is quantitatively almost 670
666 identical to that in Au+Au collisions at RHIC. We speculate 671

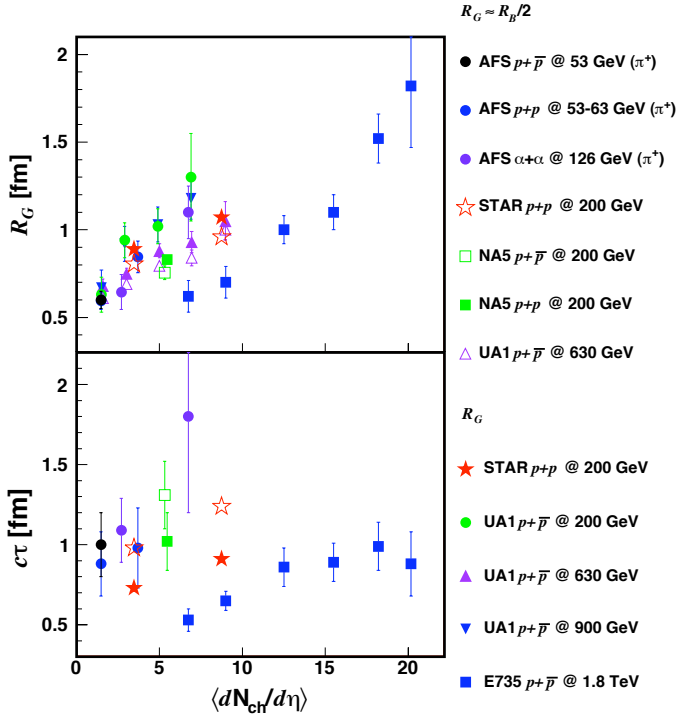


FIG. 12: (Color online) The multiplicity dependence of radius and timescale parameters to 2-dimensional correlation functions measured by STAR, E735 [36], UA1 [63], AFS [64] and NA5 [65]. The legend on the right indicates that the first 7 sets of datapoints come from fits to Eq. 7, in which case the parameter $R_B/2$ is plotted in the upper panel; the last 5 sets of datapoints come from fits to Eq. 8, for which R_G is plotted. As discussed in Section II A and confirmed by STAR and UA1, $R_G \approx R_B/2$. The UA1 Collaboration set $\tau \equiv 0$ in their fits.

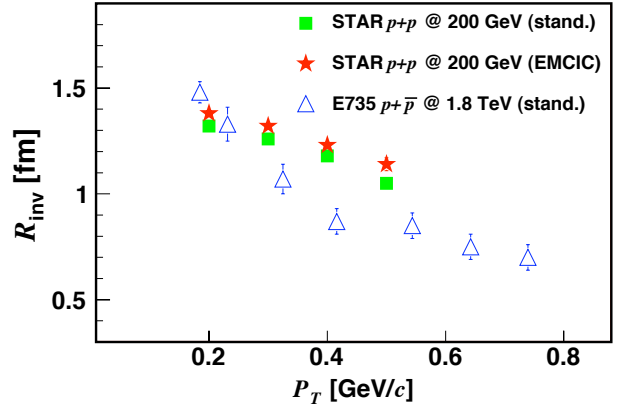


FIG. 13: (Color online) One-dimensional femtoscopic radii from $p+p$ collisions at RHIC and $p+\bar{p}$ collisions at the Tevatron [36]. are plotted versus the transverse momentum $P_T \equiv (\vec{p}_{1,T} + \vec{p}_{2,T})/2$ (c.f. Eq. 2).

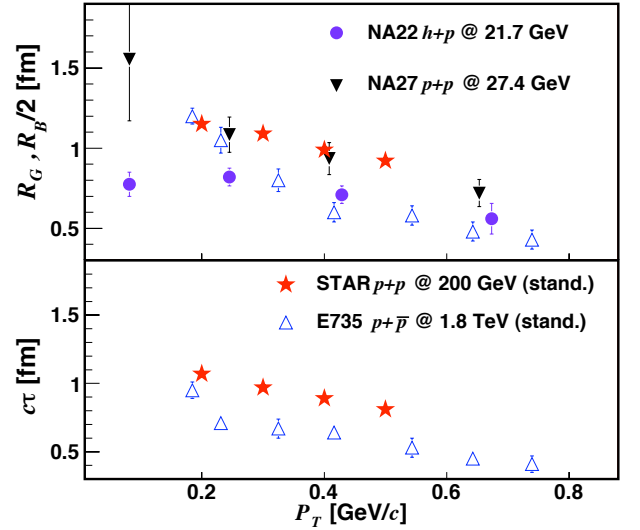


FIG. 14: (Color online) The transverse momentum dependence of fit parameters to two-dimensional correlation functions. STAR results from fit to Equation 8, compared to measurements by E735 [36], NA27 [43] and NA22 [66]. The SPS experiments NA22 and NA27 set $\tau \equiv 0$ in their fits. STAR and E735 data plotted versus $P_T \equiv (\vec{p}_{1,T} + \vec{p}_{2,T})/2$ (c.f. Eq. 2). NA27 reported results in terms of $|\vec{P}|$ and NA22 in terms of $2|\vec{P}|$. For purposes of plotting here, $P_T = \sqrt{(2/3)}|\vec{P}|$ was assumed.

702 for a fixed selection in k_T . Thirdly, the measure used to quan-
 703 tify the event multiplicity varies significantly in the historical
 704 literature; thus the determination of $\langle dN_{ch}/d\eta \rangle$ for any given
 705 experiment shown in Fig. 9 is only approximate.

706 From the discussion above, we cannot conclude definitively
 707 that there is– or is not– a universal multiplicity scaling of fem-
 708 toscopic radii in high energy hadron-hadron collisions. We
 709 conclude only that an increase of these radii with multiplicity
 710 is observed in all measurements for which $\sqrt{s} \gtrsim 40$ GeV and
 711 that the present analysis of $p+p$ collisions is consistent with
 712 world systematics.

713 In Section IV, we discussed the p_T -dependence of HBT
 714 radii observed in our analysis. Previous experiments on
 715 high-energy collisions between hadrons– and even leptons–
 716 have reported similar trends. As discussed above, direct
 717 comparisons with historical high-energy measurements are
 718 problematic. Comparisons between fit parameters to 1- and
 719 2-dimensional correlation functions are shown in Figs. 13
 720 and 14. All experiments observe a decrease in femtoscopic
 721 parameters with increasing transverse momentum. Our radii
 722 at $\sqrt{s}=200$ GeV fall off similarly or somewhat more than
 723 those measured at an order of magnitude lower energy at the
 724 SPS [30, 43], and less than those measured at an order of mag-

nitude higher energy at the Tevatron [36]. It is tempting to
 infer that this compilation indicates an energy evolution of the
 p_T -dependence of femtoscopic radii. However, given our pre-
 vious discussion, we conclude only that there is qualitative
 agreement between experiments at vastly different collision
 energies, and all show similar p_T dependence.

Systematics in 3-dimensional HBT radii from hadron col-
 lisions are less clear and less abundant, though our measure-
 ments are again qualitatively similar to those reported at the

SPS, as shown in Fig. 15. There, we also plot recent results from $e^+ + e^-$ collisions at LEP; in those 3-dimensional analyses, the “longitudinal” direction is the thrust axis, whereas the beam axis is used in hadron-hadron collisions, as in heavy ion collisions.

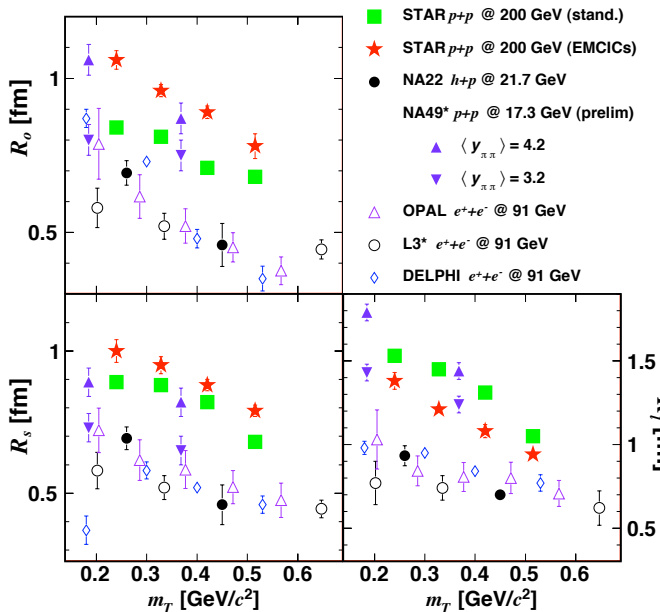


FIG. 15: (Color online) The transverse mass dependence of 3D femtoscopic radii from particle collisions. Data from NA22 [30], NA49 preliminary [67], OPAL [31], L3 [42], DELPHI [68].

VI. DISCUSSION

We have seen that HBT radii from $p + p$ collisions at RHIC are qualitatively consistent with the trends observed in particle collisions over a variety of collision energies. Further, they fall quantitatively into the much better-defined world systematics for heavy ion collisions at RHIC and similar energies. Particularly intriguing is the nearly identical dependence on m_T of the HBT radii in $p + p$ and heavy ion collisions, as this dependence is supposed [23, 69] to reflect the underlying dynamics of the latter. Several possible sources of an m_T dependence of HBT radii in small systems have been put forward to explain previous measurements.

1. Alexander *et al.* [70, 71] have suggested that the Heisenberg uncertainty principle can produce the transverse momentum dependence of femtoscopic radii in $e^+ + e^-$ collisions. However, as discussed in [20], a more detailed study of the results from $e^+ + e^-$ collisions complicates the quantitative comparisons of the data from various experiments and thus the interpretation. Additionally, the arguments from [70, 71] apply only to the longitudinal direction (R_l), so could not explain the dependence of all three radii.

2. In principle, string fragmentation should also generate space-momentum correlations in small systems, hence an

m_T dependence of the HBT radii. However, there are almost no quantitative predictions that can be compared with data. The numerical implementation PYTHIA, which incorporates the Lund string model into the soft sector dynamics, implements Bose-Einstein enhancement only as a crude parameterization designed to mock up the effect [c.f. Section 12.4.3 of 72] for the purpose of estimating distortions to W -boson invariant mass spectrum. Any Bose-Einstein correlation function may be dialed into the model, with 13 parameters to set the HBT radius, lambda parameter, and correlation shape; there is no first-principles predictive power. On more general grounds, the mass dependence of the femtoscopic radii cannot be explained within a Lund string model [73–75].

3. Long-lived resonances may also generate the space-momentum dependence of femtoscopic radii [76]. However, as discussed in [20], the resonances would affect the HBT radii from $p + p$ collisions differently than those from Au + Au collisions, since the scale of the resonance “halo” is fixed by resonance lifetimes while the scale of the “core” is different for the two cases. Thus it would have to be a coincidence that the same m_T dependence is observed in both systems. Nevertheless, this avenue should be explored further.

4. Białas *et al.* have introduced a model [73] based on a direct proportionality between the four-momentum and space-time freeze-out position; this model successfully described data from $e^+ + e^-$ collisions. The physical scenario is based on freezeout of particles emitted from a common tube, after a fixed time of 1.5 fm/c. With a very similar model, Humanic [77] was able to reproduce femtoscopic radii measured at the Tevatron [36] only with strong additional hadronic rescattering effects. With rescattering in the final state, both the multiplicity- and the m_T -dependence of the radii were reproduced [77].

5. It has been suggested [18, 30, 31, 36, 78] that the p_T -dependence of HBT radii in very small systems might reflect bulk collective flow, as it is believed to do in heavy ion collisions. This is the only explanation that would automatically account for the nearly identical p_T -scaling discussed in Section V A. However, it is widely believed that the system created in $p + p$ collisions is too small to generate bulk flow.

The remarkable similarity between the femtoscopic systematics in heavy ion and hadron collisions may well be coincidental. Given the importance of the m_T -dependence of HBT radii in heavy ion collisions, and the unclear origin of this dependence in hadron collisions, further theoretical investigation is clearly called for. Additional comparative studies of other soft-sector observables (e.g. spectra) may shed further light onto this coincidence.

VII. SUMMARY

We have presented a systematic femtoscopic analysis of two-pion correlation functions from $p + p$ collisions at RHIC. In addition to femtoscopic effects, the data show correlations due to energy and momentum conservation. Such effects have been observed previously in low-multiplicity measurements at Tevatron, SPS, and elsewhere. In order to compare to histor-

ical data and to identify systematic effects on the HBT radii, we have treated these effects with a variety of empirical and physically-motivated formulations. While the overall magnitude of the geometric scales vary with the method, the important systematics do not.

In particular, we observe a significant positive correlation between the one- and three-dimensional radii and the multiplicity of the collision, while the radii decrease with increasing transverse momentum. Qualitatively, similar multiplicity and momentum systematics have been observed previously in measurements of hadron and electron collisions at the Sp \bar{p} S, Tevatron, ISR and LEP. However, the results from these experiments could not be directly compared to those from heavy ion collisions, due to differences in techniques, fitting methods, and acceptance.

Thus, the results presented here provide a unique possibility for a direct comparison of femtoscopy in $p + p$ and $A + A$ collisions. We have seen very similar p_T and multiplicity scaling of the femtoscopic scales in $p + p$ as in $A + A$ collisions, independent of the fitting method employed. Given the importance of femtoscopic systematics in understanding the bulk sector in $Au + Au$ collisions, further exploration of the physics behind the same scalings in $p + p$ collisions is clearly important to understand our “reference” system. The similarities observed could indicate a deep connection between the underlying

physics of systems with size on order of the confinement scale, and of systems much larger. Similar comparisons will be possible at the Large Hadron Collider, where the higher collision energies will render conservation laws less important, especially for selections on the very highest-multiplicity collisions.

Acknowledgements

We thank the RHIC Operations Group and RCF at BNL, the NERSC Center at LBNL and the Open Science Grid consortium for providing resources and support. This work was supported in part by the Offices of NP and HEP within the U.S. DOE Office of Science, the U.S. NSF, the Sloan Foundation, the DFG cluster of excellence ‘Origin and Structure of the Universe’, CNRS/IN2P3, STFC and EPSRC of the United Kingdom, FAPESP CNPq of Brazil, Ministry of Ed. and Sci. of the Russian Federation, NNSFC, CAS, MoST, and MoE of China, GA and MSMT of the Czech Republic, FOM and NWO of the Netherlands, DAE, DST, and CSIR of India, Polish Ministry of Sci. and Higher Ed., Korea Research Foundation, Ministry of Sci., Ed. and Sports of the Rep. Of Croatia, and RosAtom of Russia.

-
- [1] J. Adams et al. (STAR), Nucl. Phys. **A757**, 102 (2005), nucl-ex/0501009.
- [2] K. Adcox et al. (PHENIX), Nucl. Phys. **A757**, 184 (2005), nucl-ex/0410003.
- [3] B. B. Back et al., Nucl. Phys. **A757**, 28 (2005), nucl-ex/0410022.
- [4] I. Arsene et al. (BRAHMS), Nucl. Phys. **A757**, 1 (2005), nucl-ex/0410020.
- [5] E. Schnedermann, J. Sollfrank, and U. W. Heinz, Phys. Rev. **C48**, 2462 (1993), nucl-th/9307020.
- [6] F. Retiere and M. A. Lisa, Phys. Rev. **C70**, 044907 (2004), nucl-th/0312024.
- [7] J.-Y. Ollitrault, Phys. Rev. **D46**, 229 (1992).
- [8] S. A. Voloshin, A. M. Poskanzer, and R. Snellings (2008), 0809.2949.
- [9] P. F. Kolb and U. Heinz (2003), nucl-th/0305084.
- [10] R. Lednicky, Nucl. Phys. **A774**, 189 (2006), nucl-th/0510020.
- [11] M. A. Lisa, S. Pratt, R. Soltz, and U. Wiedemann, Ann. Rev. Nucl. Part. Sci. **55**, 357 (2005), nucl-ex/0505014.
- [12] S. V. Akkelin and Y. M. Sinyukov, Phys. Lett. **B356**, 525 (1995).
- [13] R. Lednicky, V. L. Lyuboshits, B. Erazmus, and D. Nouais, Phys. Lett. **B373**, 30 (1996).
- [14] U. W. Heinz and P. F. Kolb (2002), hep-ph/0204061.
- [15] S. Pratt, Phys. Rev. **D33**, 1314 (1986).
- [16] D. H. Rischke and M. Gyulassy, Nucl. Phys. **A608**, 479 (1996), nucl-th/9606039.
- [17] S. Bekele et al. (2007), 0706.0537.
- [18] W. Kittel, Acta Phys. Polon. **B32**, 3927 (2001), hep-ph/0110088.
- [19] G. Alexander, Rept. Prog. Phys. **66**, 481 (2003), hep-ph/0302130.
- [20] Z. Chajeccki, Acta Phys. Polon. **B40**, 1119 (2009), 0901.4078.
- [21] G. I. Kopylov, Phys. Lett. **B50**, 472 (1974).
- [22] P. Jacobs and X.-N. Wang, Prog. Part. Nucl. Phys. **54**, 443 (2005), hep-ph/0405125.
- [23] S. Pratt, Phys. Rev. Lett. **53**, 1219 (1984).
- [24] G. Bertsch, M. Gong, and M. Tohyama, Phys. Rev. **C37**, 1896 (1988).
- [25] M. I. Podgoretsky, Sov. J. Nucl. Phys. **37**, 272 (1983).
- [26] P. Danielewicz and S. Pratt, Phys. Lett. **B618**, 60 (2005), nucl-th/0501003.
- [27] P. Danielewicz and S. Pratt, Phys. Rev. **C75**, 034907 (2007), nucl-th/0612076.
- [28] Z. Chajeccki and M. Lisa, Phys. Rev. **C78**, 064903 (2008), 0803.0022.
- [29] P. Avery et al. (CLEO), Phys. Rev. **D32**, 2294 (1985).
- [30] N. M. Agababyan et al. (EHS/NA22), Z. Phys. **C71**, 405 (1996).
- [31] G. Abbiendi et al. (OPAL), Eur. Phys. J. **C52**, 787 (2007), 0708.1122.
- [32] J. L. Bailly et al. (NA23), Z. Phys. **C43**, 341 (1989).
- [33] J. Uribe et al. (BNL-E766), Phys. Rev. **D49**, 4373 (1994).
- [34] R. Lednicky and M. I. Podgoretsky, Sov. J. Nucl. Phys. **30**, 432 (1979).
- [35] G. I. Kopylov and M. I. Podgoretsky, Sov. J. Nucl. Phys. **15**, 219 (1972).
- [36] T. Alexopoulos et al. (E-735), Phys. Rev. **D48**, 1931 (1993).
- [37] D. H. Boal, C. K. Gelbke, and B. K. Jennings, Rev. Mod. Phys. **62**, 553 (1990).
- [38] S. Pratt, T. Csoergoe, and J. Zimanyi, Phys. Rev. **C42**, 2646 (1990).
- [39] M. G. Bowler, Phys. Lett. **B270**, 69 (1991).
- [40] Y. Sinyukov, R. Lednicky, S. V. Akkelin, J. Pluta, and B. Erazmus, Phys. Lett. **B432**, 248 (1998).

- 927 [41] D. Buskulic et al. (ALEPH), Z. Phys. **C64**, 361 (1994). 961
- 928 [42] P. Achard et al. (L3), Phys. Lett. **B524**, 55 (2002), hep-962
ex/0109036. 963
- 930 [43] M. Aguilar-Benitez et al. (LEBC-EHS), Z. Phys. **C54**, 21 964
(1992). 965
- 932 [44] P. Abreu et al. (DELPHI), Z. Phys. **C63**, 17 (1994). 966
- 933 [45] P. Abreu et al. (DELPHI), Phys. Lett. **B286**, 201 (1992). 967
- 934 [46] Z. Chajeccki, AIP Conf. Proc. **828**, 566 (2006), nucl-968
ex/0511035. 969
- 936 [47] Z. Chajeccki and M. Lisa, Phys. Rev. **C79**, 034908 (2009),970
0807.3569. 971
- 938 [48] D. A. Brown et al., Phys. Rev. **C72**, 054902 (2005), nucl-972
th/0507015. 973
- 940 [49] W. Kittel and E. A. De Wolf (2005), *Soft Multihadron Dynam-*974
ics, Hackensack, USA: World Scientific; see especially Section975
11.5. 976
- 943 [50] C. Adler et al. (STAR), Phys. Rev. Lett. **87**, 082301 (2001),977
nucl-ex/0107008. 978
- 945 [51] J. Adams et al. (STAR), Phys. Rev. Lett. **93**, 012301 (2004),979
nucl-ex/0312009. 980
- 947 [52] J. Adams et al. (STAR), Phys. Rev. **C71**, 044906 (2005), nucl-981
ex/0411036. 982
- 949 [53] B. I. Abelev et al. (STAR), Phys. Rev. **C80**, 024905 (2009),983
0903.1296. 984
- 951 [54] M. Anderson et al., Nucl. Instrum. Meth. **A499**, 659 (2003),985
nucl-ex/0301015. 986
- 953 [55] H. Bichsel, Nucl. Instrum. Meth. **A562**, 154 (2006). 987
- 954 [56] W. M. Yao et al. (Particle Data Group), J. Phys. **G33**, 1 (2006). 988
- 955 [57] A. Kisiel and D. A. Brown (2009), 0901.3527. 989
- 956 [58] H. Caines, Eur. Phys. J. **C49**, 297 (2007), nucl-ex/0609004. 990
- 957 [59] D. Adamova et al. (CERES), Phys. Rev. Lett. **90**, 022301 991
(2003), nucl-ex/0207008. 992
- 959 [60] M. A. Lisa and S. Pratt (2008), 0811.1352.
- 960 [61] T. Alexopoulos et al. (E-735), Phys. Lett. **B528**, 43 (2002), hep-
ex/0201030.
- [62] A. Breakstone et al. (Ames-Bologna-CERN-Dortmund-
Heidelberg-Warsaw), Z. Phys. **C33**, 333 (1987).
- [63] C. Albajar et al. (UA1), Phys. Lett. **B226**, 410 (1989).
- [64] T. Akesson et al. (Axial Field Spectrometer), Phys. Lett. **B129**,
269 (1983).
- [65] C. De Marzo et al., Phys. Rev. **D29**, 363 (1984).
- [66] N. M. Agababyan et al. (EHS-NA22), Z. Phys. **C59**, 195
(1993).
- [67] R. Ganz (NA49), Nucl. Phys. **A661**, 448 (1999), nucl-
ex/9909003.
- [68] A. Smirnova (1999), *Soft Multihadron Dynamics*, Hacken-
sack, USA: World Scientific (1999) eds. N.G. Antoniou et al.,
pp.157-167.
- [69] U. W. Heinz and B. V. Jacak, Ann. Rev. Nucl. Part. Sci. **49**, 529
(1999), nucl-th/9902020.
- [70] G. Alexander, I. Cohen, and E. Levin, Phys. Lett. **B452**, 159
(1999), hep-ph/9901341.
- [71] G. Alexander, Phys. Lett. **B506**, 45 (2001), hep-ph/0101319.
- [72] T. Sjostrand, S. Mrenna, and P. Skands, JHEP **05**, 026 (2006),
hep-ph/0603175.
- [73] A. Bialas, M. Kucharczyk, H. Palka, and K. Zalewski, Phys.
Rev. **D62**, 114007 (2000), hep-ph/0006290.
- [74] G. Alexander (2001), hep-ph/0108194.
- [75] G. Alexander, Acta Phys. Polon. **B35**, 69 (2004), hep-
ph/0311114.
- [76] U. A. Wiedemann and U. W. Heinz, Phys. Rev. **C56**, 3265
(1997), nucl-th/9611031.
- [77] T. J. Humanic, Phys. Rev. **C76**, 025205 (2007), nucl-
th/0612098.
- [78] T. Csorgo, M. Csanad, B. Lorstad, and A. Ster, Acta Phys.
Hung. **A24**, 139 (2005), hep-ph/0406042.